Hindawi
Security and Communication Networks
Volume 2022, Article ID 3864480, 16 pages
https://doi.org/10.1155/2022/3864480

Research Article

Reversible Data Hiding Based on Multichannel Difference Value Ordering for Color Images

Yongjun Kong,[1] **Yan Ke**,[1,2,3] **MinQing Zhang**,[1] **TingTing Su**,[1] **Yu Ge**,[1] **and Sha Yang**[1]

[1]*Key Laboratory of Network and Information Security Under PAP, School of Cryptography Engineering in Engineering University of PAP, Xi'an, China*
[2]*Counter-terrorism Command & Information Engineering Joint Lab, Urumqi Campus of Engineering University of PAP, Urumqi, China*
[3]*Research Institute of Hi-Tech, Xi'an, China*

Correspondence should be addressed to Yan Ke; 15114873390@163.com

Received 25 April 2022; Revised 4 July 2022; Accepted 5 July 2022; Published 4 August 2022

Academic Editor: De Rosal Ignatius Moses Setiadi

Considering the correlation existing among different color channels of the image, we propose a novel reversible data hiding (RDH) scheme based on multichannel difference value ordering. By applying the technique of pixel value ordering (PVO), we establish a certain relationship by sorting the differences among adjacent pixels of different color channels. Combined with the optimized pairwise prediction-error expansion by analyzing the distribution of pixel difference, our scheme can adaptively select pixel channel to achieve reversible embedding of information. Through simulation experiments, the feasibility of this RDH scheme in image distortion and computational complexity is verified. When the threshold T is set to 3, the average PSNR of the test images embedded with 5000 bits of additional information in each color channel can reach 63.41, 64.38, and 63.96, respectively. When the embedding capacity is 20000 bits, the PSNR of the color image can reach 58.90 dB. Considering the embedding capacity and image distortion comprehensively from the simulation data, our proposed scheme has a better performance than the previous PVO-RDH schemes which only consider a single channel.

1. Introduction

Different from the traditional encryption techniques, which design high complexity encryption algorithms to convert the original data into pseudo-random coding to protect the information security, data hiding technology focuses on the construction of a hidden communication channel accompanied by a meaningful code to cover up the existence of secret data transmission to achieve the same purpose. Data hiding [1] can be divided into three categories according to different technical characteristics: steganography, digital watermark, and reversible data hiding. Steganography focuses on improving the undetectability of information embedding to resist steganography analysis. [2] Digital watermarking focuses on improving the robustness of embedded information to deal with malicious attacks in communication. [3] However, for most data hiding methods in these two categories above, unrecoverable distortion occurs which will cause permanent damage to the original carrier. In some sensitive scenarios, such permanent distortions are unacceptable, and accurate restoration of the original covering medium is required. Reversible data hiding (RDH) is a technique that can not only embed additional data into a digital medium to transfer the data through the public channel but also realize the lossless recovery of the original medium after extracting the embedded data. [4] Since RDH is characterized by nondestructive recovery after information extraction, it is more practical in image authentication [5], medical image processing [6], video error-concealment coding [7], stereo image coding [8], vector map recovery in CAD (computer-aided design) engineering graphics [9], privacy information management within hotel services [10], and other specific scenarios sensitive to data and original media. Unlike steganography, which emphasizes

undetectability, and watermarking, which emphasizes robustness, reversibility is the most important aspect of RDH. On the premise that the image can be recovered losslessly after information extraction, RDH technology is mainly studied in two aspects: improving embedding capacity and fidelity. [11, 12] Embedding capacity refers to the lossless embedding capacity of additional information for the specified embedding carrier. Fidelity refers to the similarity between the embedded image and the original image.

Among the existing RDH techniques, the method based on prediction-error expansion (PEE) has been widely studied because this method could make full use of the relevant redundancy between adjacent pixels to achieve efficient data embedding. PEE-RDH was first proposed by Thodi and Rodriguez [13], which first used PEE to create a sharp histogram and then embed secret data by extending and modifying the histogram. Since the concept of prediction error in PEE can improve the embedding performance significantly, a large number of optimization algorithms based on the method in [13] were proposed, such as building a sharper histogram by optimizing prediction accuracy [14], adaptive histogram-shifting algorithm [15], two-dimensional histogram-shifting algorithm [16], and multidimensional histogram-shifting algorithm [17].

In the process of optimizing PEE-RDH, Li proposed a high-fidelity reversible data hiding scheme based on pixel-value-ordering and prediction-error expansion. [18] The PVO method implements secret data embedding by predicting and expanding the maximum/minimum value of the second largest value/second smallest value after sorting the pixel blocks. Aided by the invariance of the pixel sequence before and after embedding, the original image can be completely restored from the marked image after extracting the embedded data. When the demand for embedded capacity is not high, PVO-RDH has better embedding performance than PEE-RDH based on other prediction methods, so it has attracted great attention. Many proposals for optimizing PVO from multiple perspectives have been proposed. In [19], after obtaining an ordered sequence, an optimized bidirectional expansion manner of the histogram is designed during the embedding process. After filtering with threshold constraints, more embedding space can be obtained, which improves the performance of the reversible data hiding scheme. In [20], the concept of Pairwise Prediction-error expansion (PPE) is introduced, and the PVO two-dimensional histogram is constructed for reversible embedding. In [21], based on the pairwise reversible embedding, a mapping optimization scheme is proposed to further improve the embedding performance. In [22], by introducing a parameter to modify the maximum/minimum value, the scheme can realize the data embedding from three directions while keeping the order unchanged so as to improve the embedding performance. In [23], by establishing the correlation between prediction-error pairs and two-dimensional histogram modification manner, an adaptive mapping selection method is proposed to realize the optimization of modification rules. In [24], by comparing the average value of the maximum pixel and minimum pixel of every sub-block, a middle pixel modification method is proposed to further improve the embedding capacity. In [25], right after nonoverlapping partition, the scheme increases/decreases the values of maximum/minimum pixels respectively so that two bins can be reserved for increasing the embedding capacity. Due to the high fidelity of PVO-RDH in a certain embedding range, it has a good embedding performance when dealing with the low embedding capacity requirements (such as instruction transmission, authentication information, and retrieval statistics) for sensitive carriers (military images, medical images, judicial images, etc.).

The previous PVO-RDH methods [18–25] that have the characteristic of high fidelity can be implemented in color images by directly applying grayscale algorithms on each channel. However, without considering the correlation among different color channels, the simple migration from three grayscale channels to a color image cannot maximize the internal redundancy. Aiming to better utilize such correlation, we propose a novel RDH scheme based on multichannel difference value ordering. Firstly, we designed a reasonable channel function, and the channel of pixel difference information is used as a reference so as to broaden the mapping coordinate space of the whole data hiding. Having done that, we associate the pixel information at the same position among multiple channels through ordering. By way of utilizing the median pixel information of three channels obtained by the adaptive selection, we also defined a computational complexity. With the defined computational complexity, we can improve the fidelity of the embedded image by constraining the embedding region according to practical requirements. What's more, to design the most efficient embedding mapping relationship, we analyze the distributions of variation trend of the differences and then took the peak area of the distributions as the center. In the available positions, an improved PPE-PVO RDH method is implemented to embed secret data. Owing to the reasonable value ordering framework among the color channel, we can realize the lossless recovery of the original information after the extraction even if the reference channel conversion occurs. Through experimental verification, the image distortion and time consumption of our scheme can meet the practical needs. Compared with the existing PVO-RDH methods based on grayscale image, the average image distortion in the three color channels is significantly reduced under the same embedding capacity verified by simulation data.

The rest of this paper is organized as follows. In Section 2, the basic knowledge of I-PVO implementation process and an optimization PVO scheme combined with PPE technology are introduced. Section 3 describes the proposed scheme based on multichannel difference value ordering in detail. Section 4 provides the experimental results that include image distortion, computational complexity analysis, embedding capacity analysis, RS steganography analysis, and performance comparisons. Finally, the conclusions are drawn in Section 5.

2. Background Knowledge

2.1. I-PVO. The PVO-RDH implements reversible embedding by adaptively selecting the embedding position based on the effective use of numerical redundancy by sorting the

pixel blocks [19]. On the basis of the original PVO, Peng introduced a new position mapping manner of the pixel sorting sequence during the embedding process and realized the bidirectional expansion of the histogram, thus optimizing the performance of the PVO-RDH algorithms.

Take the I-PVO method based on the maximum prediction in the block as an example:

(1) The two parties negotiate to divide the host image into nonoverlapping fixed-size pixel blocks.

(2) The n pixels $\{x_1, x_2, \ldots, x_n\}$ of one block is sorted to obtain an ascending sequence $\{x_{\sigma(1)}, x_{\sigma(2)}, \ldots, x_{\sigma(n)}\}$. The ascending sequence definition constraint is as follows: if $i < j$, then $x_{\sigma(i)} \le x_{\sigma(j)}$.

(3) The prediction error defined in the original PVO method merely considers the difference between the second largest value and the largest value after sorting. To obtain more embedding space, the I-PVO optimizes the prediction error combined with the position where the sorted pixel information is located. The improved prediction error is defined as

$$d = \begin{cases} x_{\sigma(n)} - x_{\sigma(n-1)}, & \text{if } \sigma(n) \ge \sigma(n-1), \\ x_{\sigma(n-1)} - x_{\sigma(n)}, & \text{otherwise.} \end{cases} \tag{1}$$

Under this definition, a nonpositive situation will occur and expansion can be performed at both sides of the histogram peak to achieve information reversible embedding.

(4) Modify the prediction error to achieve data embedding reversibly. The embedded prediction error is represented in binary form.

$$d' = \begin{cases} d + b, & \text{if } d = 1, \\ d + 1, & \text{if } d > 1, \\ d - b, & \text{if } d = 0, \\ d - 1, & \text{otherwise.} \end{cases} \tag{2}$$

The embedded pixel value $x_{\sigma(n)}{}'$ is

$$x'_{\sigma(n)} = x_{\sigma(n-1)} + |d'| = \begin{cases} x_{\sigma(n)} + b, & \text{if } d = 1, \\ x_{\sigma(n)} + 1, & \text{if } d > 1, \\ x_{\sigma(n)} + b, & \text{if } d = 0, \\ x_{\sigma(n)} + 1, & \text{otherwise.} \end{cases} \tag{3}$$

It can be inferred from (3) that the entire embedding process only performs nonsubtraction operations on the maximum value. So, the order of the original sorting sequence remains unchanged. Therefore, the reversible extraction of secret information can be implemented on the information extraction end. The specific steps are as follows:

(a) At the information extraction end, the prediction error can be obtained by the same method, and the secret information can be extracted by using

$$b = \begin{cases} d' - 1, & \text{if } d' = 1 \text{ or } d' = 2, \\ -d', & \text{if } d' = 0 \text{ or } d' = -1. \end{cases} \tag{4}$$

(b) After extracting secret information, lossless recovery can be realized by the following equation:

$$x_{\sigma(n)} = \begin{cases} x_{\sigma(n)}{}' - b, & \text{if } d' = 1 \text{ or } d' = 2, \\ x_{\sigma(n)}{}' - 1, & \text{if } d' > 2, \\ x_{\sigma(n)}{}' - b, & \text{if } d' = 0 \text{ or } d' = -1, \\ x_{\sigma(n)}{}' - 1, & \text{otherwise.} \end{cases} \tag{5}$$

The embedding operation based on the minimum prediction is similar to that based on the maximum prediction. And the embedding performance can be improved significantly by the optimized construction of prediction error.

2.2. PPE-PVO. PPE technique can establish a two-dimensional prediction-error histogram by pairwise operation of prediction error, which can significantly improve the embedding performance compared with the traditional one-dimensional expansion scheme [20].

From (3), the entire I-PVO embedding process operates only on the maximum value, while the second largest value remains unchanged. In order to achieve pairwise operation, reference [20] defined the prediction-error pair as follows:

$$\begin{aligned} e^1_{\max} &= \begin{cases} x_{\sigma(n)} - x_{\sigma(n-2)}, & \text{if } \sigma(n) \ge \sigma(n-1), \\ x_{\sigma(n-1)} - x_{\sigma(n-2)}, & \text{otherwise,} \end{cases} \\ e^2_{\max} &= \begin{cases} x_{\sigma(n-1)} - x_{\sigma(n-2)}, & \text{if } \sigma(n) \ge \sigma(n-1), \\ x_{\sigma(n)} - x_{\sigma(n-2)}, & \text{otherwise.} \end{cases} \end{aligned} \tag{6}$$

The redefined prediction-error d can be calculated according to

$$d = e^1_{\max} - e^2_{\max}. \tag{7}$$

Under this definition, the prediction-error $\{d | d \in \{0, 1\}\}$ can be directly extended to the prediction-error pair $\{(e^1_{\max}, e^2_{\max}) | e^1_{\max} - e^2_{\max} \in \{0, 1\}\}$. Figure 1 is the diagram of a two-dimensional reversible mapping of the I-PVO scheme.

During the I-PVO embedding process, $e^1_{\max}$ and $e^2_{\max}$ only be expanded related to $x_{\sigma(n)}$ while the other prediction error remains unchanged. In [20], based on the fact that the sorting sequence is not changed, the pairwise error expansion can be introduced to further improve the embedding performance.

According to Equations (6) and (7), the scheme performs adaptive type optimization classification of embedding type according to the characteristics of prediction-error pairs histogram. The classification rules are as follows:

(a) Type A : $(e^1_{\max} = 0, e^2_{\max} = 0)$ or $(e^1_{\max} = 1, e^2_{\max} = 0)$

(b) Type B : $(e^1_{\max} = 2, e^2_{\max} = 2)$

(c) Type C : $(e^1_{\max} \ge 2, e^2_{\max} = 1)$ or $(e^1_{\max} = 1, e^2_{\max} \ge 2)$

(d) Type D : $(e^1_{\max} = 1, e^2_{\max} = 1)$

(e) Type E : $(e^1_{\max} \ge 2, e^2_{\max} = 0)$ or $(e^1_{\max} = 0, e^2_{\max} \ge 1)$

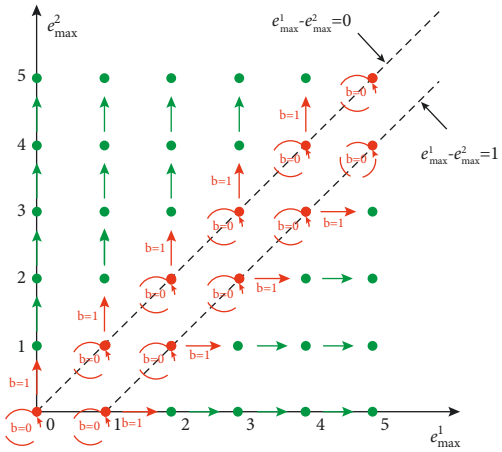

Figure 1: Two-dimensional reversible mapping.

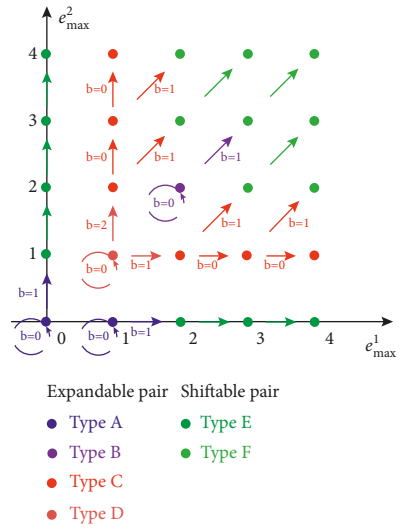

Figure 2: PPE-PVO two-dimensional reversible mapping.

(f) Type F : $(e^1_{max} \geq 2, e^2_{max} \geq 3)$ or $(e^1_{max} \geq 3, e^2_{max} \geq 2)$

In order to make full use of the prediction-error pairs from neighbor pixels $(e^1_{max} = 1, e^2_{max} = 1)$, Type A, Type B, Type C, and Type D prediction-error pairs are used as expandable pairs. Then, the pairwise expansion operations on $x_{\sigma(n)}$ and $x_{\sigma(n-1)}$ are performed under the premise of reversibility:

$$\left(x'_{\sigma(n)}, x'_{\sigma(n-1)}\right) = \left(x_{\sigma(n)}, x_{\sigma(n-1)}\right) + \left(e^1_{max}, e^2_{max}\right). \quad (8)$$

Figure 2 is a diagram of a two-dimensional reversible mapping of PPE-PVO. For different types of error pairs, according to their original characteristics, a feasible one-to-many mapping arrow expansion direction is designed to realize secret information embedding. Take Type A marked in blue as an example: when the embedded information is 0, the pixel prediction pairs keep unchanged; when the embedded information is 1, the predicted maximum value of the block will be modified by no more than 1, that is, (e^1_{max}, e^2_{max}) is expanded from $(0, 0)$ to $(1, 1)$.

3. Multichannel Difference Value Ordering

The existing PVO-RDH researches mainly focus on the single-channel gray image embedding scheme. If the embedded carrier is replaced by multichannel color images, the existing methods can only achieve reversible embedding by converting multichannel information dimension reduction into single-channel information. The multichannel feature of the color image cannot be utilized, and the redundant space between channels is wasted. In order to make better use of redundant space, a reversible data hiding scheme based on multichannel difference value ordering (MDVO) is proposed.

Color images are usually obtained by a combination of R (red), G (green), and B (blue) digital information channels. Figure 3 shows the multichannel pixel information of the color image Lena. In the specified pixel position of the color image, the pixel information between channels is generally different, but the variation trend has a certain correlation.

In order to make full use of the correlation between the trend of channel variation, multichannel differences of adjacent pixel positions are used for sorting operations to obtain the complexity of a given color pixel block to determine whether it is embedded. Finally, the reversible embedding of information is realized by defining a sorting difference extension pair.

3.1. Variable Definition. Since there are many variables involved in this scheme, for better understanding, Table 1 lists the variables of this scheme.

To select available positions for embedding, the complexity of embedding $NL_{i,j}$ is defined. $NL_{i,j}$ of the color image in specified pixel position $\text{Location}_{i,j}$ is calculated from pixels in $\text{Location}_{i,j}$, $\text{Location}_{i+1,j}$, and $\text{Location}_{i+2,j}$.

Definition 1. To distinguish the information carried by different channels, the channel label function $\text{Channel}(x)$ is introduced: when the operation pixel information x is located in the channel R, then $\text{Channel}(x) = 1$; when located in the channel G, then $\text{Channel}(x) = 2$; when located in channel B, then $\text{Channel}(x) = 3$.

First, differential values are calculated from adjacent pixels of the three channels to obtain a trend difference sequence $D_{i,j}$ and $D_{i+1,j}$, which are calculated as follows:

$$D_{i,j} = \left\{R_{i,j} - R_{i+1,j}, G_{i,j} - G_{i+1,j}, B_{i,j} - B_{i+1,j}\right\}, \quad (9)$$

$$D_{i+1,j} = \left\{R_{i+1,j} - R_{i+2,j}, G_{i+1,j} - G_{i+2,j}, B_{i+1,j} - B_{i+2,j}\right\}. \quad (10)$$

Among them, $R_{i,j}$, $G_{i,j}$, and $B_{i,j}$, respectively, represent pixel values of corresponding channels at $\text{Location}_{i,j}$.

Definition 2. The sorting function is performed on the sequence: $x = \{x_1, x_2, x_3\}$ composed of the value x_i from channels R, G, and B. The function is aimed to obtain an ascending sequence: $sort(\boldsymbol{x}) = \left\{x_{\sigma(1)}, x_{\sigma(2)}, x_{\sigma(3)}\right\}$. The ascending sequence definition constraint is as follows: if $i < j$, then $x_{\sigma(i)} \leq x_{\sigma(j)}$, and when $x_{\sigma(i)} = x_{\sigma(j)}$, then ascending

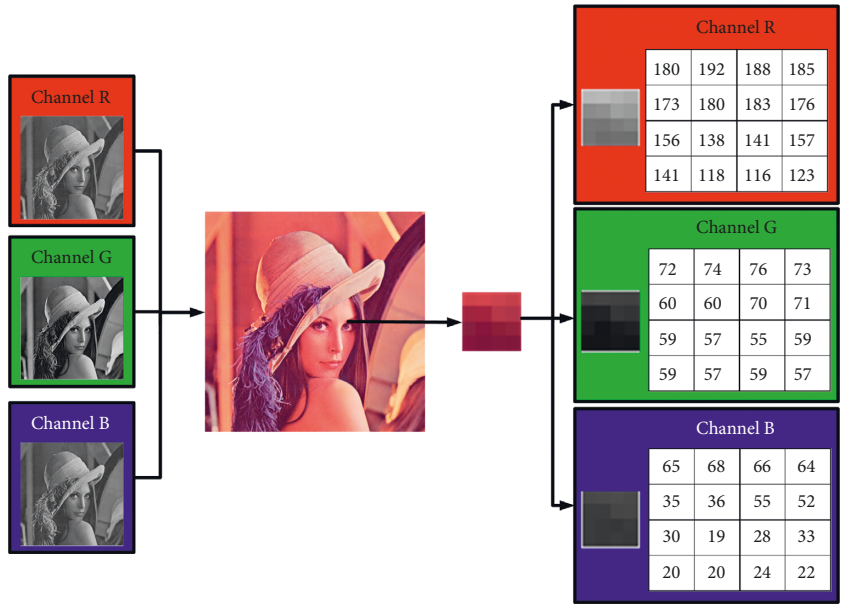

Figure 3: Lena standard color image multichannel digital information.

Table 1: Variable table.

Variable name	Description
$Location_{i,j}$	Location of pixel at row i and column j
$R_{i,j}G_{i,j}B_{i,j}$	Specify pixel information of R, G, and B channels in pixel positions i, j
$x_{\sigma(n)}$	The nth number after sorting in sequence x
$D_{i,j}$	Specify interchannel trend difference sequence of pixel positions i, j
$NL_{i,j}$	Specify interchannel complexity of pixel locations i, j
$LM_{i,j}$	Specify overflow processing flag of pixel position i, j
$(e_{\max}, e_{\min})$	Maximum value prediction-error pair information before embedding
$(e'_{\max}\, e'_{\min})$	Maximum value prediction-error pair information after embedding

sequence continues to be arranged according to the value of the channel function $\text{Channel}(x)$.

Definition 3. The median of the sorted trend differences is then used to obtain the complexity $NL_{i,j}$:

$$NL_{i,j} = \left|\left(D_{i,j}\right)_{\sigma(2)} - \left(D_{i+1,j}\right)_{\sigma(2)}\right|. \tag{11}$$

To ensure low distortion after embedding, a complexity threshold T is introduced: the available position for embedding must meet the constrain: $NL_{i,j} \le T$.

During embedding, no modification occurs on the complexity $NL_{i,j}$ to ensure the reversibility of extraction. In our scheme, the pixel values at $\text{Location}_{i+1,j}$ are only for reference. And for $\text{Location}_{i,j}$, only the pixels of the most value channel will be adaptively selected to implement error expansion up to 1 without affecting the complexity $NL_{i,j}$.

When we extend the pixel value of $\text{Location}_{i,j}$ for information hiding, the pixels at $\text{Location}_{i+1,j}$ and $\text{Location}_{i+2,j}$ need to be used for the complexity $NL_{i,j}$ calculation according to equations (10)–(12). Therefore, the traversal constraint is as follows: $1 \le i \le \text{width} - 2$ and $1 \le j \le \text{height}$, and width and height, respectively, represent the original image size. During the traversal process, if the pixel in a channel is 0 or 255, an overflow may occur during the extension process. Then, the auxiliary map LM is established. If $LM_{i,j} = 1$, it indicates that overflow occurs, otherwise mark $LM_{i,j} = 0$. The processes of the proposed scheme are as shown in Figure 4, where the orange arrow is the traversal direction.

In a pixel location $\text{Location}_{i,j}$ meeting the embedding condition, the pixel is adaptively modified in the corresponding channel of the maximum value among the three-channel differences according to the sequence $\text{sort}(D_{i,j})$. Pairwise expansion is performed on the maximum value prediction-error pair based on multichannel difference value ordering to realize data hiding.

Definition 4. Maximum value prediction-error pair based on multichannel difference value ordering is defined as follows:

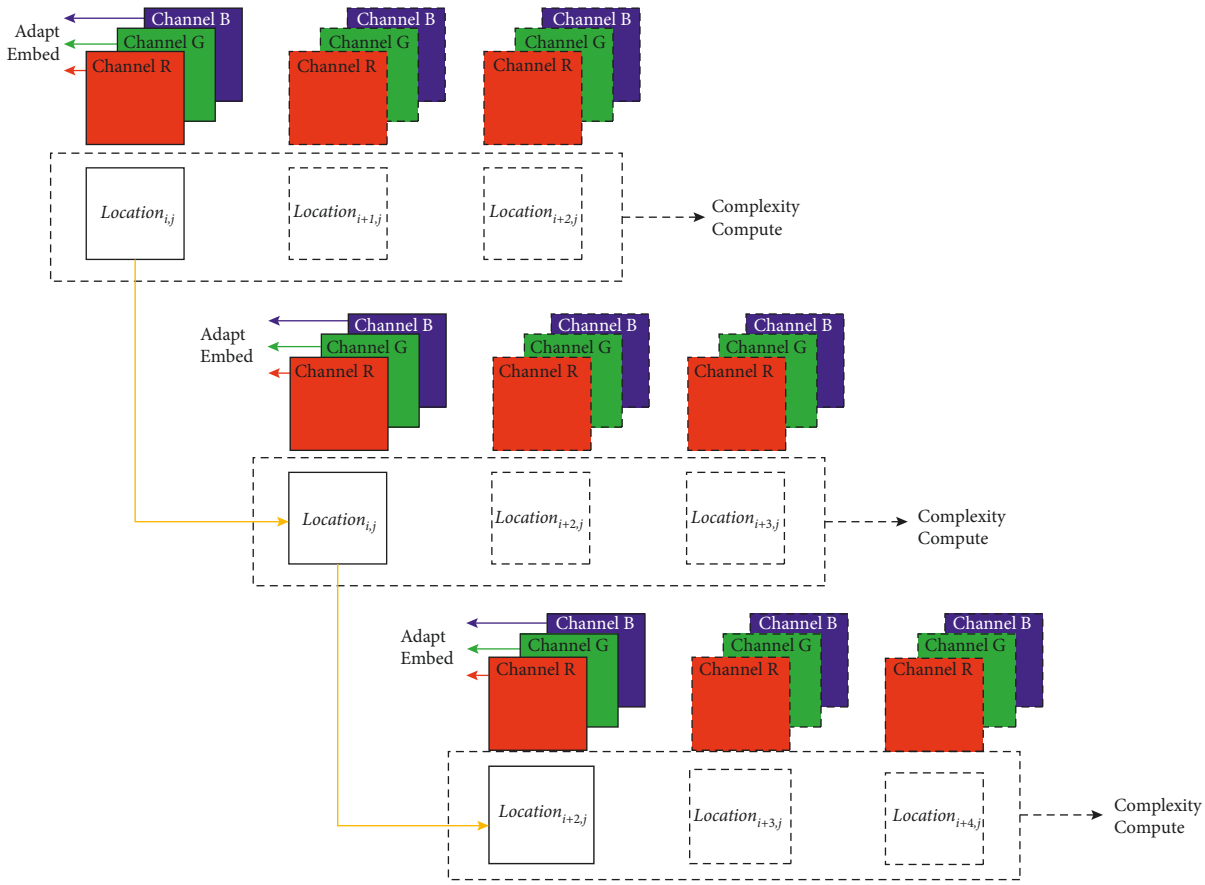

Figure 4: Traversal processes of embedding in the proposed scheme.

$$e_{\max} = \begin{cases} \left(D_{i,j}\right)_{\sigma(3)} - \left(D_{i,j}\right)_{\sigma(2)}, & \text{if Channel}\left(\left(D_{i,j}\right)_{\sigma(3)}\right) \geq \text{Channel}\left(\left(D_{i,j}\right)_{\sigma(2)}\right), \\ \left(D_{i,j}\right)_{\sigma(2)} - \left(D_{i,j}\right)_{\sigma(3)}, & \text{otherwise}, \end{cases} \tag{12}$$

$$e_{\min} = \begin{cases} \left(D_{i,j}\right)_{\sigma(2)} - \left(D_{i,j}\right)_{\sigma(1)}, & \text{if Channel}\left(\left(D_{i,j}\right)_{\sigma(2)}\right) \geq \text{Channel}\left(\left(D_{i,j}\right)_{\sigma(1)}\right), \\ \left(D_{i,j}\right)_{\sigma(1)} - \left(D_{i,j}\right)_{\sigma(2)}, & \text{otherwise}. \end{cases} \tag{13}$$

Under the above Definitions, Figure 5 shows the overall flowchart of data embedding. For the specific pixel position Location$_{i,j}$ of the original image to be embedded, the trend differences $D_{i,j}$ and $D_{i+1,j}$ are firstly calculated, and then, the complexity $NL_{i,j}$ to determine whether it is embedded or not is calculated. For the pixel position that meets the complexity threshold, if there is no overflow, the corresponding embedding operation is carried out by modifying the pixels $R_{i,j}$, $G_{i,j}$, and $B_{i,j}$ of this specific location. Follow this process to traverse all pixel positions, and finally, get the image embedded with secret information. The specific embedding operations will be described in detail in the following sections.

3.2. Data Embedding. When the complexity threshold T is set to 2, the distribution of maximum value prediction-error pair of the color image Lena is as shown in Figure 6. As can be seen from Figure 6, the value of $(e_{\max}, e_{\min})$ will be nonpositive, and the most value prediction-error pair will concentrate at (0,0), (0,1), (1,0), and (1,1). To take full advantage of the correlation of most value pairs, we extend the PPE-PVO two-dimensional mapping limited to the first quadrant to the entire two-dimensional space.

Figure 7 shows the invertible mapping relationship of the Max/Min prediction-error pairs based on multichannel difference value ordering. Based on this mapping relationship, $e_{\max} \longrightarrow e'_{\max}$ and $e_{\min} \longrightarrow e'_{\min}$ when data hiding occurs.

In the proposed scheme, the error pair of the whole two-dimensional space is divided into multiple types. Type A, Type B, and Type C can be used for reversible data hiding while Type D is only extended to ensure lossless recovery after information extraction. Based on the mapping

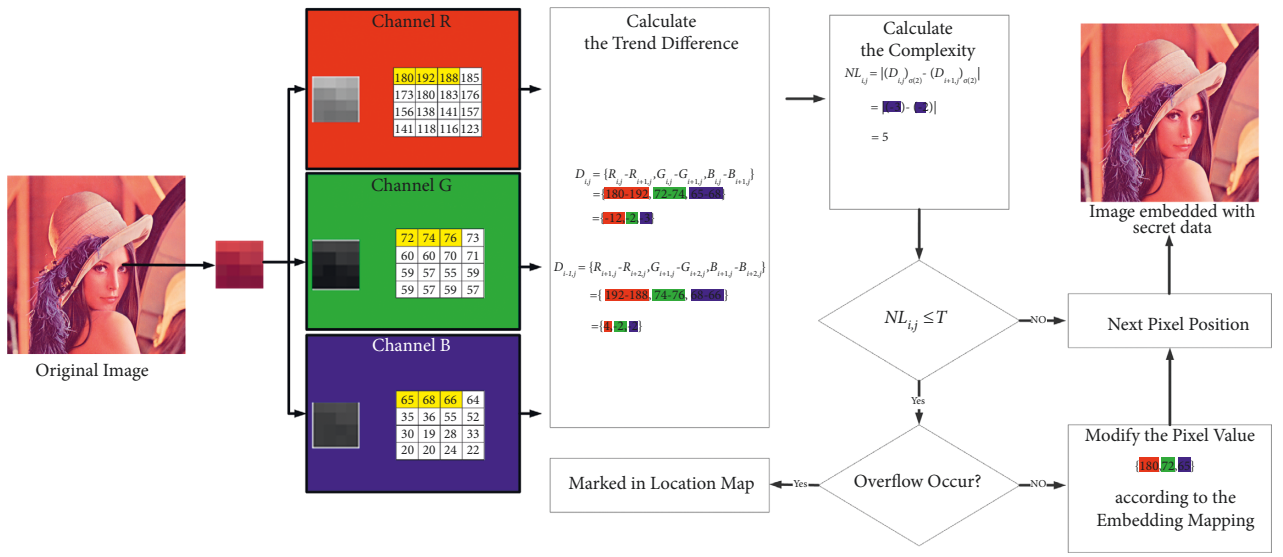

Figure 5: The overall flowchart of data embedding.

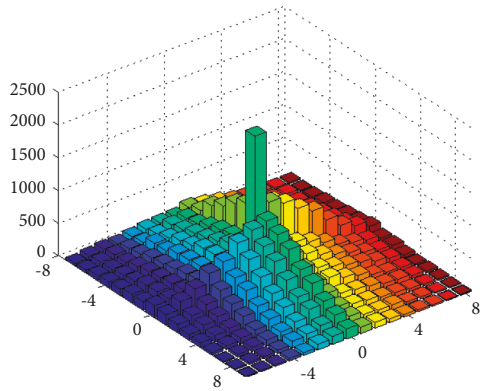

Figure 6: Most value prediction-error pair distribution histogram based on multichannel difference value ordering.

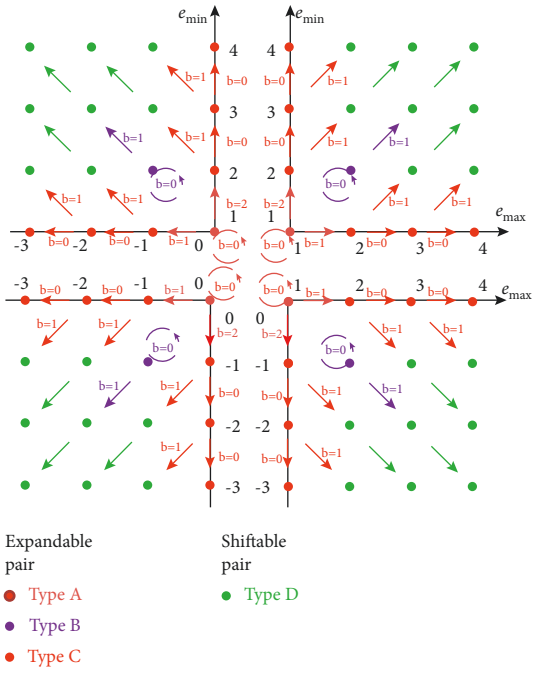

Figure 7: MDVO Max/Min prediction-error pairs embedded mapping.

relationship in Figure 6, the scheme uses the channel function to adaptively select the channel with the maximum difference among channels R, G, and B as the embedded channel. Then, we perform the reversal difference expansion to carry the additional data. The modification amplitude on the difference is within 1:

(a) When $e_{\max} = 0 \longrightarrow e'_{\max} = -1$, the expansion of most value prediction-error pair is

$$\begin{cases} \left(D_{i,j}\right)'_{\sigma(1)} = \left(D_{i,j}\right)_{\sigma(2)} - \left|e'_{\min}\right|, \\ \left(D_{i,j}\right)'_{\sigma(2)} = \left(D_{i,j}\right)_{\sigma(2)} + 1, \\ \left(D_{i,j}\right)'_{\sigma(3)} = \left(D_{i,j}\right)_{\sigma(3)} = \left(D_{i,j}\right)_{\sigma(2)}. \end{cases} \tag{14}$$

(b) When $e_{\min} = 0 \longrightarrow e_{\min}{}' = -1$, the expansion of most value prediction-error pair is

$$\begin{cases} \left(D_{i,j}\right)'_{\sigma(1)} = \left(D_{i,j}\right)_{\sigma(1)} = \left(D_{i,j}\right)_{\sigma(2)}, \\ \left(D_{i,j}\right)'_{\sigma(2)} = \left(D_{i,j}\right)_{\sigma(2)} - 1, \\ \left(D_{i,j}\right)'_{\sigma(3)} = \left(D_{i,j}\right)_{\sigma(2)} + \left|e'_{\max}\right|. \end{cases} \tag{15}$$

(c) Under other circumstances,

$$\begin{cases} \left(D_{i,j}\right)'_{\sigma(1)} = \left(D_{i,j}\right)_{\sigma(2)} - \left|e_{\min}\right|, \\ \left(D_{i,j}\right)'_{\sigma(2)} = \left(D_{i,j}\right)_{\sigma(2)}, \\ \left(D_{i,j}\right)'_{\sigma(1)} = \left(D_{i,j}\right)_{\sigma(2)} + \left|e_{\max}\right|. \end{cases} \tag{16}$$

Finally, the reversible embedding of secret information is achieved by using channel information of adjacent reference locations.

$$\begin{cases} R'_{i,j} = \left(D_{i,j}\right)'_{\sigma(a)} + R_{i+1,j}\left(\text{channel}\left(\left(D_{i,j}\right)'_{\sigma(a)}\right) = 1\right), \\ G'_{i,j} = \left(D_{i,j}\right)'_{\sigma(b)} + G_{i+1,j}\left(\text{channel}\left(\left(D_{i,j}\right)'_{\sigma(b)}\right) = 2\right), \\ B'_{i,j} = \left(D_{i,j}\right)'_{\sigma(c)} + B_{i+1,j}\left(\text{channel}\left(\left(D_{i,j}\right)'_{\sigma(c)}\right) = 3\right). \end{cases} \tag{17}$$

3.3. Extraction and Recovery. During the embedding process, the complexity values of the MDVO sequence keep unchanged. Therefore, the solution can directly perform the inverse traversal of the entire color image from the back to the front to extract the secret information and the lossless recovery of the image.

Auxiliary information such as overflow markers and thresholds is pretransmitted by existing side information processing strategies. For the pixel positions satisfying the complexity threshold and $LM_{i,j} = 0$, the most value prediction-error pair $e_{\max}{}'$ and $e_{\min}{}'$ is calculated by (12) and (13). As shown in Figure 8, the data extraction and the reversible recovery of prediction-error pair can be implemented. The two recovery processes, which are from $e_{\max}{}'$ to $e_{\max}$ and from $e_{\min}{}'$ to $e_{\min}$, are carried out according to the specific mapping relationships of MVDO.

In the image recovery process, since there is no mapping process from 0 to −1, the situation of multichannel difference jump between channels is avoided. The recovery of Max/Min pair from multichannel difference value ordering is performed by using the median value that remains constant during embedding:

$$\begin{cases} \left(D_{i,j}\right)_{\sigma(1)} = \left(D_{i,j}\right)'_{\sigma(2)} - \left|e_{\min}\right|, \\ \left(D_{i,j}\right)_{\sigma(2)} = \left(D_{i,j}\right)'_{\sigma(2)}, \\ \left(D_{i,j}\right)_{\sigma(3)} = \left(D_{i,j}\right)'_{\sigma(2)} + \left|e_{\max}\right|. \end{cases} \tag{18}$$

Finally, the recovery of the original pixels of the three channels is achieved by using the channel information of the adjacent reference positions:

$$\begin{cases} R_{i,j} = \left(D_{i,j}\right)_{\sigma(a)} + R_{i+1,j}\left(\text{channel}\left(\left(D_{i,j}\right)'_{\sigma(a)}\right) = 1\right), \\ G_{i,j} = \left(D_{i,j}\right)_{\sigma(b)} + G_{i+1,j}\left(\text{channel}\left(\left(D_{i,j}\right)'_{\sigma(b)}\right) = 2\right), \\ B_{i,j} = \left(D_{i,j}\right)_{\sigma(c)} + B_{i+1,j}\left(\text{channel}\left(\left(D_{i,j}\right)'_{\sigma(c)}\right) = 3\right). \end{cases} \tag{19}$$

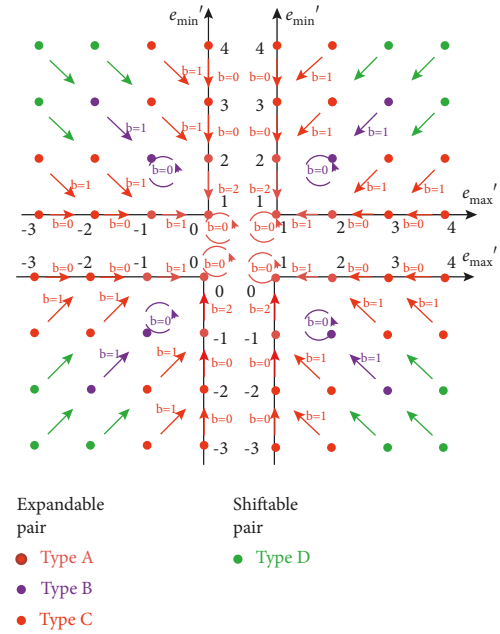

Figure 8: MDVO Max/Min prediction-error pairs extraction and recovery mapping.

3.4. Embedding and Extraction Example. As is shown in Figure 9, it is an example of the proposed RDH scheme based on MVDO under the condition of the complexity constraint allows. In Figure 9, from left to right, there are the original differences of each channel, the embedded differences of each channel, and the recovered differences of each channel. The color of red, green, and blue, respectively, represents the channel that the pixel differences belong to.

In the processes of the first row, the pixel differences from the red, green, and blue channels are 2, 4, and 3, respectively. As the difference value of blue channel is determined to be the median value after sorting, the blue channel is used as the reference channel according to Definition 1. Then, the difference of the other two channels is predicted to obtain the corresponding interchannel prediction-error pair (−1, 1). If the to-be-embedded bit is 0, the prediction-error pair is modified into (−2, 1) according to the mapping relationship illustrated in Figure 6. The difference of the reference channel is kept unchanged, and the difference of the other two channels is modified according to the modification rule. The embedded differences of the red, green, and blue channels are obtained as (2, 5, 3).

During the extraction, the blue channel is determined as the reference channel by the same sorting operation. The prediction-error pair (−2, 1) is obtained. Then, according to the mapping relationship illustrated in Figure 7, the embedded bit 0 is extracted and the prediction-error pair can be restored to (−1, 1). The differences of the red, green, and blue channels are restored to (2, 4, 3). The pixels can also be restored according to the modification rule. The other pixel difference groups in the first column represent the different information hiding process under different mappings and different embedded bit. Especially for the fourth row, when the mapping relationship changes from 0 to −1, the

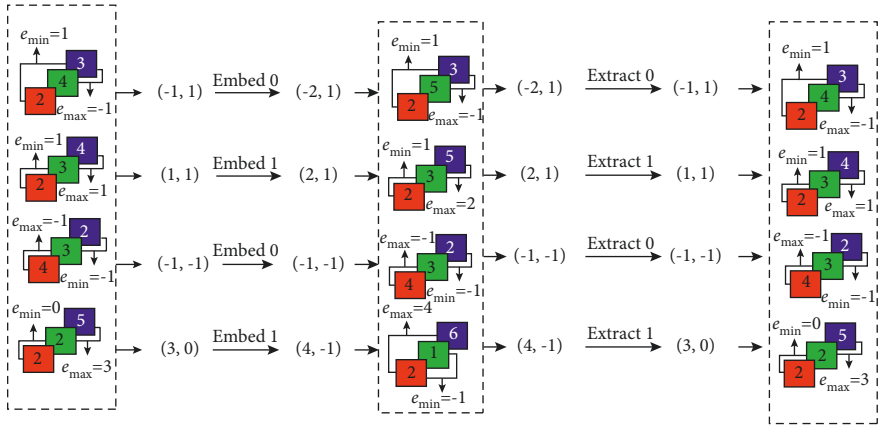

Figure 9: MDVO embedding and extraction process.

conversion of the reference channel will occur without changing the value of the reference channel. During the whole operation, the pixel values of each channel are modified and restored according to the unprocessed pixel values and the corresponding differences by using (17) and (19). Simulation results show that the whole information hiding process can ensure the reversibility of the original carrier.

3.5. Main Contributions. With the continuous development of communication hardware and network technology, color images instead of gray images have become the main digital carrier of social communication and replace gray images. Starting from the characteristics of color image and combined with PVO technology, the proposed scheme has the following contributions:

(a) A reasonable channel function is designed, and the channel of pixel difference information is used as a reference so as to broaden the mapping coordinate space of the whole information hiding.

(b) Based on the redundancy of adjacent pixels in the same channel, the pixel information at the same position among multiple channels is associated by sorting.

(c) The computational complexity is calculated by using the pixel information of the median channel obtained by adaptive selection so that the area to be embedded can be constrained according to the embedding needs to improve the image quality.

(d) Analyze the distributions of variation trend of the differences and then take the peak area of the distributions as the mapping center so as to design the most efficient information embedding mapping relationship.

(e) By ordering the value difference among the color channels, even if the reference channel conversion occurs, the lossless recovery of the original information can still be realized after the information extraction.

4. Experiments and Analysis

To verify the performance of the proposed RDH scheme, we demonstrate the experimental results of six standard color images from the USC-SIPI image library as shown in Figure 10. All the experiments were implemented on the MATLAB2018a with 64-bit single-core CPU (i7-6800K) @ 3.40 GHz WINDOWS10 system for simulation.

4.1. Distortion in MDVO Channel. The Peak Signal Noise Ratio (PSNR) is generally used as an image distortion measure to analyze the image quality after embedding.

$$PSNR(I', I) = 10 * \log_{10}\left(\frac{(2^n - 1)^2}{MSE(I\prime, I)}\right). \tag{20}$$

For grayscale images with a color depth of 8 bits, $\mathrm{MSE}_{\mathrm{gray}}$ indicates the mean square error of the pixel value of the embedded image and the original image. The definition of the single-channel gray image is as shown in the following equation:

$$MSE_{\mathrm{gray}}(I', I) = \frac{\sum_{i=0}^{M-1}\sum_{j=0}^{N-1}\left(I_{i,j}' - I_{i,j}\right)^2}{M \times N}. \tag{21}$$

The definition of the multichannel color image is shown in the following equation:

$$MSE_{\mathrm{color}}(I', I) = \frac{\sum_{\mathrm{channel}}^{R,G,B}\sum_{i=0}^{M-1}\sum_{j=0}^{N-1}\left(I_{i,j}^{\mathrm{channel}\prime} - I_{i,j}^{\mathrm{channel}}\right)^2}{M \times N \times 3}. \tag{22}$$

During the simulation experiment, the threshold T was set to 3. Figure 11 shows the overall distortion of the image and the distortion of each channel under the certain embedded capacity of the test image. In Figure 11, black spots represent the PSNR of the color image, while red, green, and blue spots represent the PSNR of the image from different channels, respectively.

Compared with channel R or channel B, the median of multichannel difference sorting appears most frequently in channel G. In most cases, no modification takes place in a

Figure 10: Six standard color images for testing. (a) Tiffany; (b) airplane; (c) lake; (d) peppers; (e) baboon; (f) Splash.

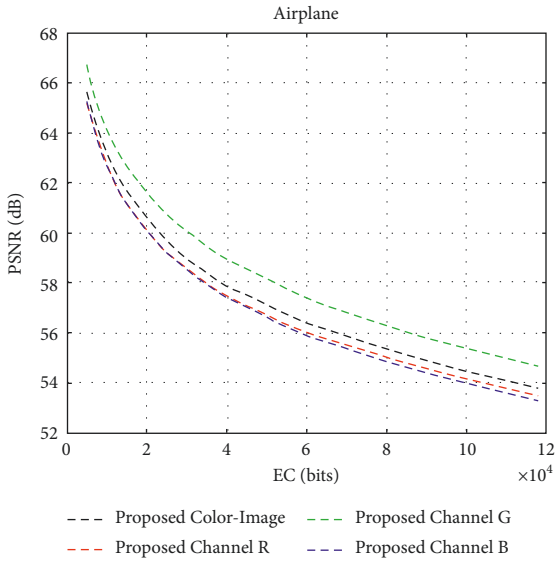

Figure 11: Image Airplane and channel distortion.

reference channel. It can be seen from Table 2 that when the embedding capacity is increased from 5000 bits to 20000 bits, the average PSNR of the channel G is 0.95 dB and 0.53 dB higher than that of channel R and channel B, respectively, which indicates that the image quality of the channel G is the best. In practical applications, the embedded color image may be transmitted in the form of a grayscale image. The color image information is generally converted from RGB to YUV space, and then, the brightness information Y is represented as a single channel of the color image. The conversion formula is as follows:

$$Y = 0.299 \times R + 0.587 \times G + 0.114 \times B. \quad (23)$$

In (23), when the color image is transmitted in a public channel in the form of brightness information, channel G information contributes the most. The proposed RDH method could adaptively select the corresponding channel for embedding by sorting, which would better reduce the information distortion in channel G compared with the other two channels. Therefore, the scheme can better ensure the high quality of the embedded color image when transmitting in the grayscale channel of the common channel.

4.2. Computational Complexity Analysis. To verify the practicability of the proposed scheme, we will analyze the computational complexity from the view of complexity theory. For a color image with the size of width and height, n pixel positions can be used for information embedding, where n is equal to width − 2 times height. For a specified position $\text{Location}_{i,j}$ to be embedded, which can be inferred from Definition 1 in Section 3, there are 9-pixel values from different channels at two adjacent pixel positions which need

Table 2: The PSNR (dB) of different channels in color image.

	PSNR (EC = 5000 bit)				Average PSNR (EC = 5 000-20 000 bit)			
Image	Color	Red	Green	Blue	Color	Red	Green	Blue
Tiffany	63.96	64.45	63.48	64.00	60.41	61.16	59.94	60.23
Airplane	65.66	65.16	66.73	65.27	62.61	62.15	63.71	62.16
Lake	63.82	62.78	64.35	64.55	61.16	60.18	61.81	61.67
Pepper	62.85	62.27	63.59	62.81	59.34	58.73	60.03	59.35
Baboon	60.98	60.25	62.33	60.63	60.08	59.42	61.38	59.67
Splash	65.91	65.53	65.77	66.48	62.16	61.68	62.12	62.75
Average	63.86	63.41	64.38	63.96	60.96	60.55	61.50	60.97

Table 3: Execution Time (ms) of complexity calculation for different images.

Image	Maximum consumption	Minimum consumption	Average consumption
Tiffany	2074.81	1560.01	1670.93
Airplane	2199.61	1575.61	1686.37
Lake	2418.02	1544.41	1672.95
Peppers	2262.01	1560.01	1665.93
Baboon	2168.41	1544.41	1665.31
Splash	1872.01	1560.01	1642.69

to be subtracted 6 times to obtain trend difference sequences $D_{i,j}$ and $D_{i+1,j}$. The computational complexity of this step is $o(6n)$. Then, according to Definition 2, the median channels $(D_{i,j})_{\sigma(2)}(D_{i+1,j})_{\sigma(2)}$ can be obtained by ordering the channel differences at the same position with an order length of 3. This operation can be replaced by three subtraction operations, that is, the computational complexity of this step is $o(3n) + o(3n)$. Finally, the median channels of the target position and the reference position are compared, and then, the absolute value is taken to obtain the parameter $NL_{i,j}$ of the position $\text{Location}_{i,j}$. In the simulation process, the operation of taking the absolute value compares the difference between the value and zero and then determines whether to take the inverse. The computational complexity of this step is $o(2n)$. Therefore, the computational complexity of acquiring all parameters $NL_{i,j}$ is $o(13n)$.

Under the hardware and software conditions shown above, Figure 11 and Table 3 illustrate the time consumption obtained after calculating complexity parameters $NL_{i,j}$ of the six test images 100 times. The acquisition method of time consumption comes from the function cpu-time of platform MATLAB. The abscissa of Figure 12 represents the execution label of every simulation, and the ordinate represents the specific execution time of every simulation. The maximum, minimum, and average consumptions obtained from executing 100 simulation experiments of every image are shown in Table 3. According to the experimental data, for our scheme, the image texture has little effect on the time consumption in the complexity calculation process. During the simulation process, the time consumption is between 1560.01 and 2418.02 milliseconds, and the average time consumption is 1667.36 milliseconds, which can meet the needs of practical applications.

This scheme can adjust the complexity threshold T to meet different embedding requirements and then adaptively select better embedding positions through the comparison between T and $NL_{i,j}$. The modified channel and the modification method can be determined according to the MDVO mapping relationship. The complexity of the entire modification operation increases linearly with the increase of embedding capacity, and the time consumption is quite small compared with the complexity calculation.

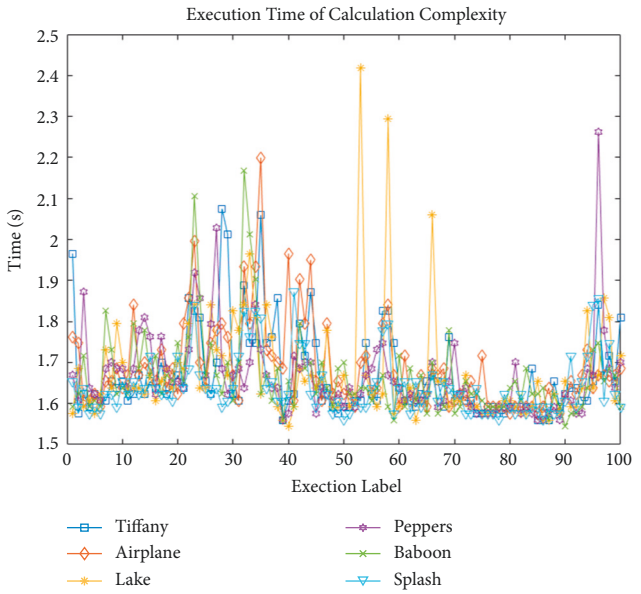

Figure 12: Execution time.

4.3. Embedding Capacity Analysis. The embedding performance of this scheme is related to the adjacent complexity between image channels. The average image complexity is obtained by calculating the average values of all pixel positions according to equations (9), (10), and (11). The specific calculation formula is as follows:

$$NL_{\text{Image}} = \sum_{i=1}^{M-2} \sum_{j=1}^{N} NL_{i,j}. \tag{24}$$

Table 4: Maximum embedded capacity (bits) of different images.

Image	Complexity	Peng et al. [19]	Ou et al. [20]	He et al. [21]	Haldar et al. [23]	Wu et al. [24]	Kumal et al. [25]	$T=1$	$T=2$	$T=3$	$T=4$	$T=5$
Tiffany	5.11	42000	46000	47000	49000	47000	76000	47000	61000	72000	81000	87000
Airplane	6.46	48000	50000	52000	58000	62000	91000	68000	98000	118000	132000	142000
Lake	12.87	26000	29000	29000	40000	29000	34000	13000	20000	26000	31000	35000
Peppers	8.34	30000	35000	36000	37000	36000	42000	18000	24000	30000	35000	41000
Baboon	29.68	13000	14000	14000	12000	14000	22000	—	5000	7000	9000	11000
Splash	4.23	46000	49000	51000	54000	61000	88000	66000	93000	111000	124000	132000

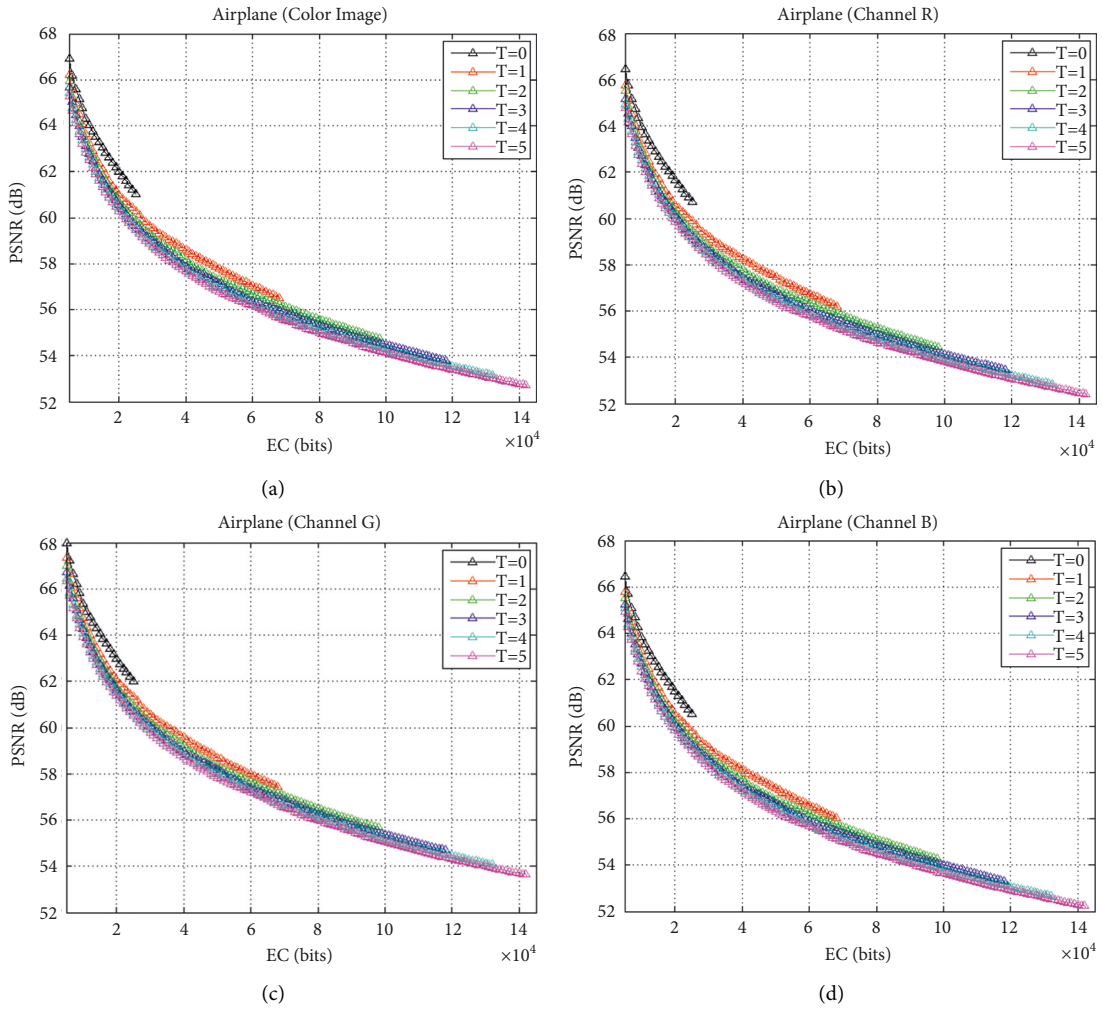

Figure 13: Airplane embedding capacity—PSNR under different thresholds. (a) Color; (b) red channel; (c) green channel; (d) blue channel.

As can be seen from Table 4, the interchannel complexity of the image is inversely proportional to the embedding capacity. As for an image with higher complexity between channels, it could provide a less embedding capacity under the same threshold setting.

In the preprocessing stage, PVO-RDH methods filter the embedding space by using the complexity threshold and only expand the pixel position with high redundancy space so as to greatly improve the fidelity of the embedded image. When the complexity threshold is set to be bigger than 5, the maximum embedding capacity of this scheme is close to that of most existing PVO methods. With the threshold getting larger or the filtering constraints getting less, the maximum embedding capacity would get further improved.

It can be seen from Figure 13, under the same embedding capacity, the distortion will be larger as the threshold increases. According to Figure 14, it can also be obtained that the PSNR of the image airplane embedded with 20000 bits of additional data is 61.99 dB when the threshold is 0. When the threshold is set to 5, PSNR is 58.32 dB. Therefore, in practice, the threshold setting should consider both the capacity and image quality requirements.

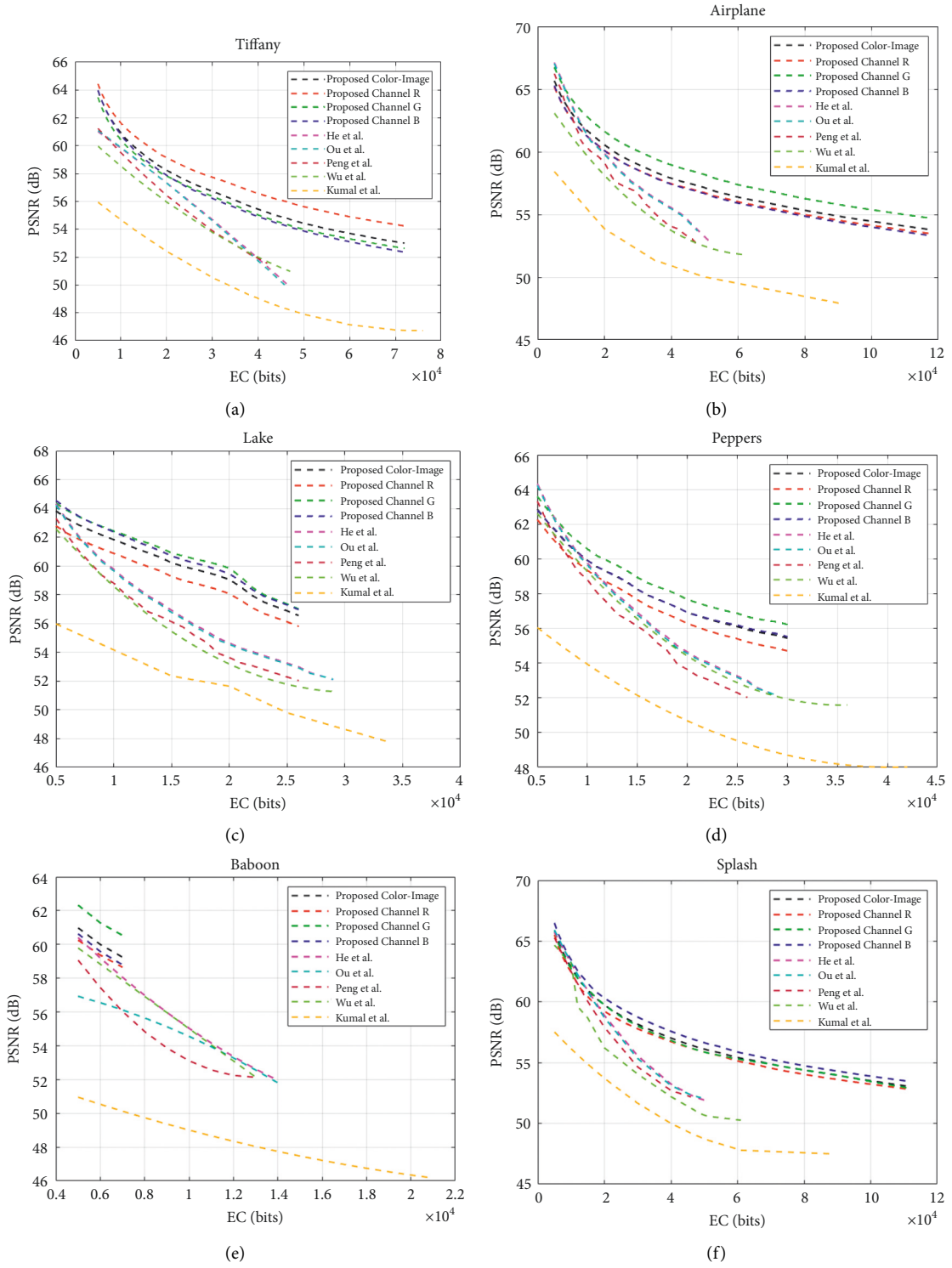

Figure 14: Embedded capacity—PSNR. (a) Tiffany; (b) airplane; (c) lake; (d) peppers; (e) baboon; (f) splash.

4.4. RS Steganography Analysis. From the MDVO Max/Min prediction-error pairs embedded mapping as shown in Figure 7, we can conclude that the embedding operation only changes the pixel value with an amplitude less than 1. In this way, only the least significant and second least significant bits will change. Therefore, we use the RS analysis method [26] for LSB statistics of spatial images to implement steganography analysis.

Function $f(x_1, \ldots, x_n)$ represents the correlation of a pixel group $\{x_1, \ldots, x_n\}$:

Table 5: RS analysis results of different images.

Image		R_M	R_{-M}	S_M	S_{-M}	$R_M - S_M$	$R_{-M} - S_{-M}$
Tiffany	Channel R	24432	24512	19288	19143	5144	5369
	Channel G	24664	24702	19335	19304	5329	5398
	Channel B	24454	24539	19256	19135	5198	5404
Airplane	Channel R	24459	24325	19456	19351	5003	4974
	Channel G	24766	24595	19535	19412	5231	5183
	Channel B	24553	24431	19402	19259	5151	5172
Lake	Channel R	24084	24314	19243	19293	4841	5021
	Channel G	24553	24631	19351	19359	5202	5272
	Channel B	23799	23968	19195	19205	4604	4763
Peppers	Channel R	24351	24402	19261	19084	5090	5318
	Channel G	24827	24902	19353	19288	5474	5614
	Channel B	24481	24608	19291	19102	5190	5506
Baboon	Channel R	23516	23322	19123	19146	4393	4176
	Channel G	23996	23822	19172	19282	4824	4540
	Channel B	23571	23378	19129	19150	4442	4228
Splash	Channel R	24760	24702	19331	19321	5429	5381
	Channel G	24811	24680	19550	19451	5261	5229
	Channel B	24656	24566	19366	19290	5290	5276

$$f(x_1, \ldots, x_n) = \sum_{i=1}^{n-1} |x_{i+1} - x_i|. \tag{25}$$

Flip Function F:

$$\begin{aligned} F_1&: 0 \leftrightarrow 1, 2 \leftrightarrow 3, \ldots, 252 \leftrightarrow 253, 254 \leftrightarrow 255 \\ F_{-1}&: -1 \leftrightarrow 0, 1 \leftrightarrow 2, \ldots, 255 \leftrightarrow 256 \\ F_0&: F(x) \leftrightarrow x. \end{aligned} \tag{26}$$

According to the above functions, a pixel group $G = \{x_1, \ldots, x_n\}$ can be divided into three categories:

$$\begin{aligned} &G \in Rf(F(G)) > f(G), \\ &G \in Sf(F(G)) < f(G), \\ &G \in Uf(F(G)) = f(G). \end{aligned} \tag{27}$$

When the pixel group size n is set to 4, the masks used in the simulation are $M = (1, 0, 1, 0)$ and $-M = (-1, 0, -1, 0)$. The RS analysis results obtained by f our proposed scheme under the condition that the threshold T was set to 3 are shown in Table 5, where R_M, R_{-M}, S_M, and S_{-M} represent the occurrences of different pixel groups with different masks M and $-M$ according to equations (25), (26), and (27).

In the preprocessing stage, our proposed scheme adaptively selects pixel positions with high correlation to achieve reversible data hiding through the constraint of the threshold T. In addition, according to the prediction-error pairs embedded mapping, additional information can be embedded in some pixel positions even without modifying any pixel values. As can be observed directly from Table 5, the rules $R_M \cong R_{-M}$ and $S_M \cong S_{-M}$ can be satisfied in different color channels of different images. What's more, we further analyzed the difference value $R_M - S_M$ and $R_{-M} - S_{-M}$, and these two statistics are also very similar. Therefore, we can conclude that our proposed method can resist RS steganography.

4.5. Distortion and Embedding Capacity. The PVO-RDH scheme can set the corresponding threshold according to the embedding requirements, and the pixel position can be adaptively selected by the threshold. Therefore, under low embedding capacity, the embedding performance of the RDH scheme is better than that of other unconditional constrained RDH schemes. This paper mainly refers to the idea of the numerical ordering in PVO, realizes efficient embedding under threshold constraint, and designs RDH scheme based on MDVO according to the multichannel characteristics of the color image. Compared with the existing PVO schemes (e.g., Peng et al. [19], Ou et al. [20], He et al. [21], Wu et al. [24], and Kumal et al. [25]), this scheme has better embedding performance on the PSNR of the embedded images for RDH applications that use color images as the carrier.

The existing PVO-RDH methods are all for grayscale images, in which the difference extension was performed in a single grayscale channel. The proposed scheme utilizes the correlation of pixels between channels to sort multichannel differences with redundancy, and then, the optimal channel is adaptively selected for reversible embedding. When information embedding is performed, the value of the sorted median channel does not change when it is used as a reference channel. At the same time, the modification is adaptively selected according to the reversible embedding mapping in the other two channels. The pixel distortion caused by the information embedding in this scheme will spread to three channels. Therefore, the PSNR of the channels R, G, and B under this scheme is significantly higher than that of the single-channel PVO-RDH.

The embedded operation of the specified image channel may be identified in the public transmission channel. Therefore, the image distortion in a single channel should be reduced as much as possible while realizing the specified embedding capacity. As can be seen from Table 6, when the embedding capacity is 20000 bits, the PSNR of the color

Table 6: Comparison of PSNR (dB) of the embedded images at EC = 10000, 20000 bit.

Image	Peng et al. [19]	Ou et al. [20]	He et al. [21]	Wu et al. [24]	Kumal [25]	Proposed color	Proposed red	Proposed green	Proposed blue
EC = 10 000 bit									
Tiffany	58.83	59.48	59.58	58.76	53.82	60.93	61.64	60.43	60.80
Airplane	63.06	63.76	63.85	61.35	56.90	63.16	62.69	64.26	62.70
Lake	58.80	59.66	59.78	58.79	53.97	61.83	60.87	62.42	62.37
Peppers	58.90	59.32	59.41	59.66	54.16	59.92	59.34	60.57	59.92
Baboon	54.71	54.56	53.33	55.01	49.13	—	—	—	—
Splash	62.87	63.45	63.55	63.22	56.32	62.86	62.45	62.72	63.47
Average	59.53	60.04	59.92	59.00	53.36	61.74	61.40	62.08	61.85
EC = 20 000 bit									
Tiffany	57.63	57.58	57.32	56.89	52.46	58.24	59.14	57.83	57.88
Airplane	59.86	59.79	59.14	57.85	53.86	60.56	60.12	61.63	60.09
Lake	54.65	54.56	53.64	53.12	50.74	59.06	58.07	59.85	59.45
Peppers	55.32	55.23	54.82	54.42	51.64	56.92	56.28	57.66	56.92
Baboon	—	—	—	—	—	—	—	—	—
Splash	58.23	58.19	57.93	56.22	52.77	59.75	59.24	59.76	60.32
Average	57.13	57.07	56.57	55.70	52.29	58.90	58.57	59.35	58.93

image reaches 58.90 dB. The channel R with the largest degree of distortion in multichannel pixel information is improved by 1.77, 1.83, 2.33, 3.20, and 6.61 dB, respectively, compared with the existing PVO schemes of Peng et al. [19], Ou et al. [20], He et al. [21], Wu et al. [24], and Kumal et al. [25].

5. Conclusion

This paper concentrates to improve the fidelity of the marked image after RDH by using the correlation among pixels at the same position of different color channels. Firstly, we propose the channel function in Definition 1 to achieve subsequent channel selection among the three color channels. The complexity in Definition 3 is proposed to select low-complexity pixels for embedding. Difference pairs among the pixels and their adjacent ones are calculated for adaptively ordering in Definition 4. After the above preprocessing calculation of the image, two-dimensional reversible embedding map is designed by analyzing the difference distribution among multichannels. Based on the Max/Min value prediction-error pairs of MDVO, additional data could be embedded according to the proposed embedding map. Through simulation experiments and theoretical analysis, we verified the feasibility of image distortion and computational complexity of our proposed scheme. Since PVO technology is firstly proposed to be associated with the channel variation trend of the color image, experimental results demonstrate that the largest degree of distortion is still improved by 1.77, 1.83, 2.33, 3.20, and 6.61 dB, respectively, compared with the existing PVO schemes of Peng et al. [19], Ou et al. [20], He et al. [21], Wu et al. [24], and Kumal et al. [25]. Therefore, this study is of great significance to applications that need to deliver retrieval messages or authentication messages in sensitive scenarios such as military communications, medical management, and judicial forensics.

Reversible information hiding mainly focuses on the lossless recovery of the original carrier, so it is generally transmitted in a trusted channel without considering malicious attacks. This scheme can improve the fidelity of the image while ensuring reversible embedding. In this scheme, the embedding of a large amount of additional information cannot be satisfied due to the threshold condition. In the future, further research can be studied on the usage of the color channel information to establish high-dimensional redundancy or establish multiple embedding rules so as to improve the embedding capacity to meet the needs of practical RDH applications.

Data Availability

Key codes and parameter settings used to support the findings of the study are included within the article.

Disclosure

The author would like to declare on behalf of the coauthors that the work described was original research that has not been published previously, and not under consideration for publication elsewhere, in whole or in part.

Conflicts of Interest

No conflicts of interest exist in the submission of this manuscript.

Authors' Contributions

All the authors listed have approved the manuscript that is enclosed.

Acknowledgments

This work was supported by Natural Science Foundation of China, under Grant nos. 62102450, 62102451, and 61872384, and fundamental research fund project of Engineering University of PAP, under Grant no. WJY202112.

References

[1] Y. Q. Shi, X. Li, X. Zhang, H. T. Wu, and B. Ma, "Reversible data hiding: a," *IEEE Access*, vol. 4, pp. 3210–3237, 2016.

[2] A. K. Sahu and M. Sahu, "Digital image steganography and steganalysis: a journey of the past three decades," *Open Computer Science*, vol. 10, no. 1, pp. 1–47, 2020.

[3] A. Gutub, "Watermarking images via counting-based secret sharing for lightweight semi-complete authentication," *International Journal of Information Security and Privacy*, vol. 16, no. 1, pp. 1–18, 2022.

[4] Z. Ni, Y. Q. Shi, N. Ansari, and W. Su, "Reversible data hiding," *IEEE Transactions on Circuits and Systems for Video Technology*, vol. 16, no. 3, pp. 354–362, 2006.

[5] C. W. Honsinger, P. W. Jones, M. Rabbani, and J. C. Stoffel, "Lossless recovery of an original image containing embedded data," US6278791B1, 2001.

[6] G. Coatrieux, C. Le Guillou, J. M. Cauvin, and C. Roux, "Reversible watermarking for knowledge digest embedding and reliability control in medical images," *IEEE Transactions on Information Technology in Biomedicine*, vol. 13, no. 2, pp. 158–165, 2008.

[7] K. L. Chung, Y. H. Huang, P. C. Chang, and H. Y. M. Liao, "Reversible data hiding-based approach for intra-frame error concealment in H.264/AVC," *IEEE Transactions on Circuits and Systems for Video Technology*, vol. 20, no. 11, pp. 1643–1647, 2010.

[8] D. Coltuc and I. Caciula, "Stereo Embedding by Reversible Watermarking: Further results," in *Proceedings of the 2009 International Symposium on Signals, Circuits and Systems*, pp. 1–4, IEEE, Iasi, Romania, July 2009.

[9] F. Peng, Y. Lei, M. Long, and X. M. Sun, "A reversible watermarking scheme for two-dimensional CAD engineering graphics based on improved difference expansion," *Computer-Aided Design*, vol. 43, no. 8, pp. 1018–1024, 2011.

[10] A. K. Sahu and A. Gutub, "Improving grayscale steganography to protect personal information disclosure within hotel services," *Multimedia Tools and Applications*, pp. 1–21, 2022.

[11] A. K. Sahu and G. Swain, "High fidelity based reversible data hiding using modified LSB matching and pixel difference," *Journal of King Saud University - Computer and Information Sciences*, vol. 34, no. 4, pp. 1395–1409, 2022.

[12] F. S. Hassan and A. Gutub, "Efficient reversible data hiding multimedia technique based on smart image interpolation," *Multimedia Tools and Applications*, vol. 79, pp. 30087–30109, 2020.

[13] D. M. Thodi and J. J. Rodriguez, "Expansion embedding techniques for reversible watermarking," *IEEE Transactions on Image Processing*, vol. 16, no. 3, pp. 721–730, 2007.

[14] X. Hu, W. Zhang, and N. Yu, "Optimizing Pixel Predictors Based on Self-Similarities for Reversible Data hiding," in *Proceedings of the 2014 Tenth International Conference on Intelligent Information Hiding and Multimedia Signal Processing*, pp. 481–484, IEEE, Kitakyushu, Japan, August 2014.

[15] H. Chen, J. Ni, W. Hong, and T. S. Chen, "Reversible data hiding with contrast enhancement using adaptive histogram shifting and pixel value ordering," *Signal Processing: Image Communication*, vol. 46, pp. 1–16, 2016.

[16] P. H. Vo, T. S. Nguyen, V. T. Huynh, and T.-N. Do, "A novel reversible data hiding scheme with two-dimensional histogram shifting mechanism," *Multimedia Tools and Applications*, vol. 77, no. 21, pp. 28777–28797, 2018.

[17] J. Zhao and Z. Li, "Three-dimensional histogram shifting for reversible data hiding," *Multimedia Systems*, vol. 24, no. 1, pp. 95–109, 2018.

[18] X. Li, J. Li, B. Li, and B. Yang, "High-fidelity reversible data hiding scheme based on pixel-value-ordering and prediction-error expansion," *Signal Processing*, vol. 93, no. 1, pp. 198–205, 2013.

[19] F. Peng, X. Li, and B. Yang, "Improved PVO-based reversible data hiding," *Digital Signal Processing*, vol. 25, no. 2, pp. 255–265, 2014.

[20] B. Ou, X. Li, and J. Wang, "High-fidelity reversible data hiding based on pixel-value-ordering and pairwise prediction-error expansion," *Journal of Visual Communication and Image Representation*, vol. 39, pp. 12–23, 2016.

[21] W. G. He, G. Q. Xiong, S. W. Weng, Z. Cai, and Y. Wang, "Reversible data hiding using multi-pass pixel-value-ordering and pairwise prediction-error expansion," *Information Sciences*, vol. 467, pp. 784–799, 2018.

[22] S. Meikap and B. Jana, "Directional PVO for reversible data hiding scheme with image interpolation," *Multimedia Tools and Applications*, vol. 77, no. 23, pp. 31281–31311, 2018.

[23] A. Haldar, S. De, and B. Jana, "Pixel value ordering with prediction error expansion based high fidelity reversible data hiding scheme," *International Journal of Applied Engineering Research*, vol. 14, no. 4, pp. 997–1005, 2019.

[24] H. Wu, X. Li, Y. Zhao, and R. Ni, "Improved reversible data hiding based on PVO and adaptive pairwise embedding," *Journal of Real-Time Image Processing*, vol. 16, no. 3, pp. 685–695, 2019.

[25] R. Kumar, N. Kumar, and K. H. Jung, "I-PVO based high capacity reversible data hiding using bin reservation strategy," *Multimedia Tools and Applications*, vol. 79, no. 8, pp. 22635–22651, 2020.

[26] J. Fridrich, M. Goljan, and D. Rui, "Reliable detection of LSB steganography in color and grayscale images," *Mm & Sec Proceedings of the Workshop on Multimedia & Security New Challenges*, vol. 8, pp. 22–28, 2002.